STOCHASTIC COOLING AND RELATED RF COMPONENTS

F. Nolden
Gesellschaft für Schwerionenforschung, Planckstraße 1, D-64291 Darmstadt, Germany

Abstract
This paper describes some of the pick-up and kicker structures that are currently in use for stochastic cooling. The emphasis is on the general physical properties of the devices.

1 QUALITATIVE INTRODUCTION TO STOCHASTIC COOLING

Stochastic cooling is a powerful method of decreasing the phase space volume of coasting beams. Invented by Simon van der Meer in 1969, the first successful cooling experiments were performed in the 1970s at CERN. Important physics experiments such as the detection of the W and Z bosons at CERN and the top quark at Fermilab depended crucially on the stochastic cooling of antiproton beams which were needed in colliders like the SPS and the Tevatron. An extensive bibliography can be found in Dieter Möhl's lecture at the 1993 CERN accelerator school [1]. Nowadays, the scope of stochastic cooling has been extended to different particles and different laboratories, such as proton cooling at COSY [2] and heavy ions at GSI (Darmstadt) [3]. A radioactive beam facility with stochastic cooling is planned at RIKEN in Tokyo [4].

The principal idea of stochastic cooling is to make use of the information inherent in the fluctuations of a coasting beam, in order to derive a correction signal which is applied to the beam very shortly after detection. These fluctuations are unavoidable because beams consist of a finite number of particles. The signal is detected by pick-up electrodes, processed in order to extract the desired information (momentum deviation or transverse emittance), amplified and transmitted to kicker electrodes, where the properties of the beam are changed in order to decrease the phase space volume. The kick is applied in the same revolution as the signal is detected. The principal layout of a stochastic cooling system is shown in Fig. 1. For an introduction to the physics of stochastic cooling, the reader should refer again to Ref. [1].

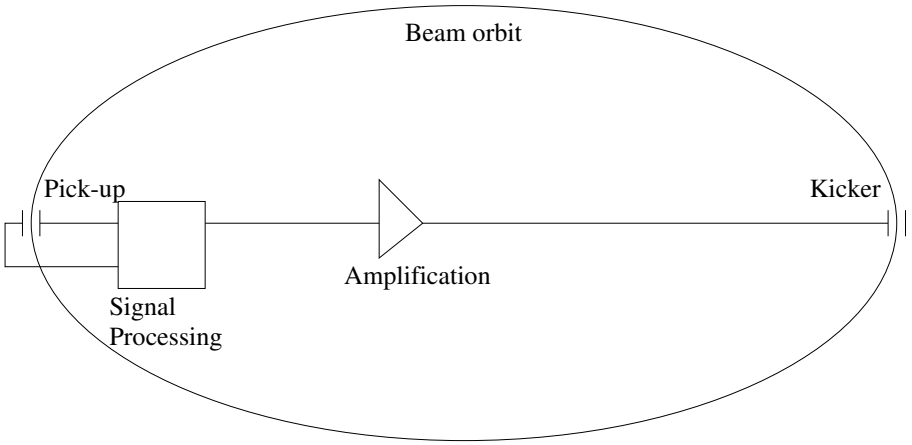

Fig. 1: Principal layout of a stochastic cooling system.

An important figure of merit for the quality of the signal as well as the efficiency of the cooling system is the temporal resolution of signal detection. The higher the resolution, the smaller are the parts of the beam to be observed simultaneously and the more informative is the fluctuating signal. Because of the uncertainty relation between the time and the frequency domains, a high temporal resolution is

equivalent to a large frequency bandwidth W. Indeed, it can be shown rather easily that the optimum cooling rate $1/\tau$ of a stochastic cooling system is $2W/N$, where N is the number of particles in the beam.

In order to get reasonable cooling times, practical stochastic cooling systems are usually run with bandwidths in the range 0.5–8 GHz. They are therefore based on microwave technology. Inside and outside the beam chamber, careful impedance matching is a necessary prerequisite for effective cooling. Fast signal transmission is performed either through air-filled coaxial lines, or even, if long transmission lengths are used, by optical systems [5]. Large signal amplifications > 100 dB are common and broad-band power amplifiers with good linearity needed. Travelling wave tubes are used at Fermilab, whereas amplifiers based on gallium arsenide power FET's developed for the first time at CERN [6] are common in the European laboratories. The very large bandwidths > 1 GHz are realized using several sub-bands.

Another important issue is the signal-to-noise ratio at the input port of the first (low noise) preamplifier as well as the noise figure of the preamp. The signal is proportional to the sensitivity of the pick-up structure and the noise is proportional to the effective temperature of the pick-up-preamplifier system. Expensive low-temperature systems have been built for antiproton and proton cooling systems. Even for heavy ions with their intrinsically large Schottky signals (see below) thermal cooling is being considered at GSI for second-generation machines, where very short cooling times are envisaged for rare secondary nuclear species with short half-lives.

The purpose of this paper is to present a few of the common pick-up and kicker devices and, with more emphasis, to explain some general physical relationships. It will be shown that reciprocity enables one to consider pick-up and kicker structures using a common formalism based on the notion of sensitivity. Sensitivity will be defined for the longitudinal response and this treatment will be generalized to betatron motion.

The simplest way to define sensitivity is to look at the fields excited by a kicker and calculate the integrated longitudinal field a particle experiences during passage. Later, we will show how the reciprocity theorem (or rather, the assumption of reciprocity) can be used to describe the signal induced by a particle inside a pick-up structure which is built identically. In order to calculate transverse kicks, we will apply the Panofsky–Wenzel theorem.

For a different view of the subject, the reader is referred to related lectures by C.S. Taylor [7], F. Caspers [8], G. Lambertson [9], or J. Bisognano and C. Leeman [10]. Many of the ideas presented here originate from these texts.

2 KICKERS

2.1 Sensitivity

It will be useful in the following chapters to perform some of the calculations with the vector potential $\vec{A}$, because it turns out to be very straightforward to formulate the Panofsky–Wenzel theorem with $\vec{A}$. The electric RF field is $\vec{E} = -\partial\vec{A}/\partial t$. We shall use the coordinates s, x, y for the longitudinal, horizontal, and vertical directions, and neglect effects of orbit curvature. Indeed, most of the pick-ups and kickers are installed in straight sections (an exception is the system at the ESR storage ring at GSI). Let us assume short structures where the variations of x and y are negligible during one passage. The signal at the entrance port of the device, located at s_0, can be described by a voltage $V(t)$. Inside the kicker structure there is an electromagnetic wave propagating with (positive) signal velocity v_{S}. For large particle velocities the wave is usually chosen to be counter-propagating. It gives rise to a longitudinal field component

$$A_s(s,x,y,t) = a(s,x,y)V(t \pm \frac{s-s_0}{v_{\mathrm{S}}}) \,, \tag{1}$$

where the plus sign is used for co-propagating and the minus sign for counter-propagating waves. If the velocity of the particle is v, then the integrated field seen by the particle becomes

$$\int ds A_s(s,x,y,t+\frac{s-s_0}{v}) = \int d\tau S(x,y,\tau)V(t-\tau) = S(x,y,t) * V(t) \ , \tag{2}$$

where we have introduced the sensitivity

$$S(x,y,\tau) = v_{\rm eff} a(s_0 - v_{\rm eff}\tau, x, y) \ . \tag{3}$$

The effective velocity is defined by

$$\frac{1}{v_{\rm eff}} = \frac{1}{v} \mp \frac{1}{v_S} \ . \tag{4}$$

The last equation of Eq. (2) shows that the vector potential can be calculated from the sensitivity via a convolution. Hence, with the help of the Fourier convolution theorem Eq. (A.1.8), it is easy to switch to the frequency domain where products of the Fourier transforms of S and V can be used. The reader should verify the fact that $S(x,y,t)$ is a dimensionless number. It is easy to calculate from Eq. (2) the integrated electric field:

$$\int ds E_s(s,x,y,t+\frac{s-s_0}{v}) = -\frac{\partial S(x,y,t)}{\partial t} * V(t) \ . \tag{5}$$

We therefore define a longitudinal electric sensitivity via

$$S_{\|}(x,y,t) = -\frac{\partial S(x,y,t)}{\partial t} \ . \tag{6}$$

In order to descibe spectra, later on we will need the Fourier transform $S_{\|}(x,y,\Omega)$ of $S_{\|}(x,y,t)$, which is again a dimensionless quantity.

In order to calculate the transverse kicks, we define the transverse sensitivities

$$S_x(x,y,t) = \frac{\partial S(x,y,t)}{\partial x} \tag{7}$$

$$S_z(x,y,t) = \frac{\partial S(x,y,t)}{\partial z} \ . \tag{8}$$

2.2 Electrostatic approximation

For highly relativistic beams, the electric near fields of a beam particle are disk-shaped and the sensitivity can be calculated using electrostatic field models. For kickers, Lambertson [9] has shown that the transverse variation of the accelerating voltage $U = \int E_s ds$ is governed by the equation

$$\frac{\partial^2 U}{\partial x^2} + \frac{\partial^2 U}{\partial y^2} + \frac{1}{(\beta\gamma c)^2}\frac{\partial^2 U}{\partial t^2} = 0 \ , \tag{9}$$

which looks very much like a two-dimensional Poisson equation in the relativistic limit $v \to c$. Note the appearance of the factor $1/(\beta\gamma)$ which can be attributed to the relativistic shrinking of the Coulomb field. As a typical application of Eq. (9) we calculate the field of a stripline electrode.

2.3 Stripline or quarter-wave electrode

2.3.1 Geometry of the device

A stripline electrode consists of an interruption of the upper or lower part of the vacuum chamber of width w and length L (see Fig. 2). The longitudinal electric field only penetrates into the vacuum chamber at the two ends of the device. Let us use the electrostatic approximation to derive a common model of the sensitivity. In the following, we examine this structure in some detail in order to illustrate some typical problems and applications.

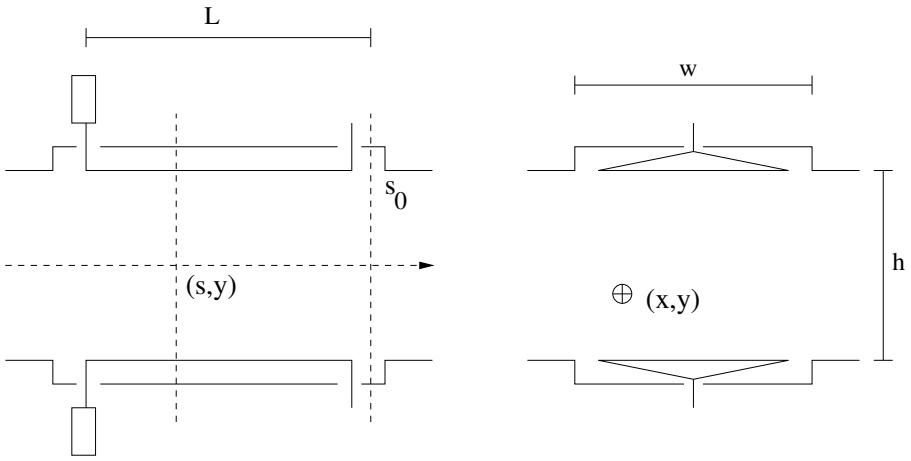

Fig. 2: Schematic sketch of a quarter-wave electrode.

2.3.2 Solution of the electrostatic problem

In order to solve the electrostatic problem, we use a simple two-dimensional model which is depicted on the left in Fig. 3. The plates of width w are symbolized by the thick lines around $x = 0$. They are at a potential V, whereas the rest of the x-axis and the parallel walls at $y = h$ are at zero potential. In order to compute the potential inside the vacuum chamber, we apply a conformal mapping. The reader who does not wish to go into the details should skip the following derivation and continue with the result in Eqs. (19) and (20). The prescription for the conformal mapping is adapted from Ref. [11]. We use complex variables $z = x + iy$ and a conformal mapping to the plane $\zeta = \xi + i\eta$ via

$$\zeta = g(z) = \exp\left(\frac{\pi z}{h}\right) . \tag{10}$$

A geometrical sketch of this mapping is shown in Fig. (3). The z-plane is shown on the left-hand side, the ζ-plane on the right-hand side. The shaded areas are potential-free. The (complex) potential in the

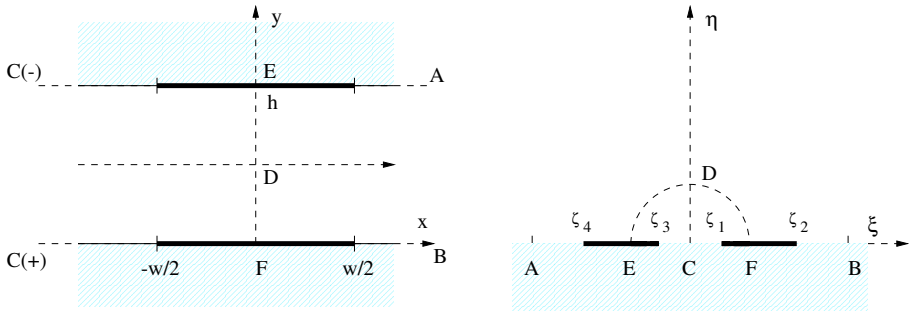

Fig. 3: Electrostatic model of quarter-wave electrode and conformal mapping.

ζ-plane is the superposition of the potentials from the upper and lower electrodes:

$$\Phi(\zeta) = \Phi_{\text{lower}}(\zeta) \pm \Phi_{\text{upper}}(\zeta) . \tag{11}$$

The positive sign is valid if the device is used as a longitudinal pick-up or kicker, i.e. if the upper and lower plates are operated in the sum mode. For operation in the difference mode (vertical pick-ups or kickers), the negative sign is valid. The constituent potentials are

$$\Phi_{\text{lower}}(\zeta) = -\frac{Vi}{\pi} \log \frac{\zeta - \zeta_1}{\zeta - \zeta_2} \tag{12}$$

$$\Phi_{\text{upper}}(\zeta) = -\frac{Vi}{\pi} \log \frac{\zeta - \zeta_4}{\zeta - \zeta_3} \tag{13}$$

with

$$\zeta_1 = g(-w/2) \tag{14}$$
$$\zeta_2 = g(w/2) \tag{15}$$
$$\zeta_3 = g(-w/2 + ih) \tag{16}$$
$$\zeta_4 = g(w/2 + ih)\ . \tag{17}$$

Because the mapping is conformal, the potentials in the z- and ζ-planes are equal, and the electric potential is

$$V(x,y) = \mathrm{Re}\left(\Phi[g(x+iy)]\right)\ . \tag{18}$$

The calculation of $V(x,y)$ from the complex functions involved is somewhat lengthy. The result is again the superposition of the two potentials

$$V(x,y) = V\sigma(x,y) = V\left(\sigma_{\mathrm{lower}}(x,y) \pm \sigma_{\mathrm{upper}}(x,y)\right)\ , \tag{19}$$

with

$$\sigma_{\mathrm{lower,upper}}(x,y) = \frac{1}{\pi}\arctan\left[\frac{\sin(\pi y/h)\sinh(\pi w/2h)}{\cosh(\pi x/h) \mp \cos(\pi y/h)\cosh(\pi w/2h)}\right]\ , \tag{20}$$

where the negative sign applies to the lower plate and the positive sign to the upper one. In the mid-plane, both potentials are equal:

$$\sigma_{\mathrm{lower}}(x,h/2) = \sigma_{\mathrm{upper}}(x,h/2) = \frac{1}{\pi}\arctan\left[\frac{\sinh(\pi w/2h)}{\cosh(\pi x/h)}\right]\ . \tag{21}$$

In the sum mode, the maximum voltage in the mid-plane is found at $x = 0$ and is $2V$ if $w \gg h$.

2.3.3 Time domain versus frequency domain picture

If an RF voltage is applied at the upstream end of the device, a wave with velocity v_{S} will propagate down the electrode and dissipate in the terminating resistor (see Fig. 2). The electric fields inside the vacuum chamber, due to a positive voltage between the electrode and the ground plane, point in opposite directions at the two ends. In order to obtain a net accelerating effect, the length of the electrode must be adapted to the beam and signal velocities in such a way that the beam particle arrives at both ends of the device at the right moment, when the wave amplitude has changed sign. We assume that the interaction time between the beam and the field at the end of the device is short compared to the characteristic time $2t_e = L/v_{\mathrm{eff}}$ (refer to Eq. (4) for the definition of v_{eff}). Then we can approximate the interaction by delta functions in the time domain and obtain for the sensitivity

$$S_{\parallel}(x,y,t) = \sigma(x,y)\left(-\delta(t) + \delta(t-2t_e)\right)\ . \tag{22}$$

The origin of time is defined such that the exciting voltage $V(t)$ is measured at the upper port of the electrode. In order to get the response in the frequency domain, one has to take the Fourier transform of Eq. (22). This is given by

$$S_{\parallel}(x,y,\Omega) = -2i\sigma(x,y)\sin(\Omega t_e)e^{-i\Omega t_e/2}\ . \tag{23}$$

Up to a phase the response is therefore essentially sinusoidal with a maximum at the frequency

$$f_{\mathrm{max}} = \frac{\Omega_{\mathrm{max}}}{2\pi} = \frac{1}{4t_e}\ . \tag{24}$$

If $v_{\mathrm{S}} = v = c$, then $f_{\mathrm{max}} = 4c/L$. The stripline electrode is therefore also called the quarter-wave electrode.

2.3.4 *Superelectrodes*

A superelectrode is generated by connecting two quarter-wave electrodes in series, with a delay $2t_e$ between the exit port of the first and the entrance port of the second one (the dashed line in Fig. 4).

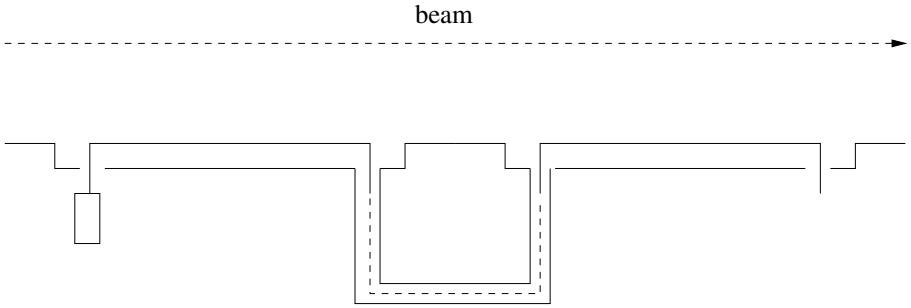

Fig. 4: Principal sketch of the lower half of a superelectrode kicker with delay line.

The sensitivity is then

$$S_{||}(x,y,t) = \sigma(x,y)\Big(-\delta(t) + \delta(t-2t_e) - \delta(t-4t_e) + \delta(t-6t_e)\Big) \tag{25}$$

with the frequency response

$$S_{||}(x,y,\Omega) = -4i\sigma(x,y)\sin(\Omega t_e)\cos(2\Omega t_e)e^{-3i\Omega t_e/2}\,. \tag{26}$$

At mid frequency, this is twice the value of a normal electrode, but the bandwidth is smaller, which can be attributed simply to the increased duration of the accelerating pulse train. Adding even more electrodes is even more obstructive to the bandwidth and has therefore never come into practice in stochastic cooling systems. Instead, power combination is used, as will be discussed later on.

2.3.5 *Finite β correction*

As can be seen from Eq. (9), the electrostatic approximation no longer holds if the beam velocity $v = \beta c$ is substantially smaller than c. As the electrostatic aproximation is intimately related to the relativistic shrinking of the Coulomb field, a generalization of the material presented above can be found in Ref. [12], where the point-like interactions in Eqs. (22) and (25) are replaced by the typical temporal variation of the Coulomb field at finite β,

$$\delta(t) \mapsto \frac{\left[1 + (t/\Delta t_{\rm pulse})^2\right]^{-3/2}}{\Delta t_{\rm pulse}}\,. \tag{27}$$

At a distance d from the particle, the finite length of the pulse is $\Delta t_{\rm pulse} = d/(\beta\gamma c)$. The Fourier transform of the right-hand side of Eq. (27) is

$$\tilde{f}(\Omega) = \Omega\Delta t_{\rm pulse}\, K_1(\Omega\Delta t_{\rm pulse})\,, \tag{28}$$

where K_1 is a modified Bessel function. In order to make the finite β correction effective, the idealized frequency response of Eqs. (23) and (26) must be multiplied by $\tilde{f}(\Omega)$. The effect of the correction is always a reduced sensitivity compared with the case $v = c$. Some estimates are given in Ref. [12]. This simple correction comes close to the results of sophisticated field theoretical models [13].

2.4 Planar loops

Planar loops [14] have been used extensively in the Fermilab stochastic cooling systems. They are fabricated completely with the microstrip line technique. The ground plane of the microstrip plate is cut in order to interrupt the image current of the particle [see Fig. 5]. On the opposite side, where the microstrips are situated, there is a tapered connection [the dashed trapezoid in Fig. 5] from the 50 Ω signal line. A hole is drilled through the dielectric in order to produce a galvanic connection between the end of the tapered microstrip and the 'electrode'. The electrode itself can be interpreted as a 100 Ω structure. On the other side of the 'electrode', a terminating resistor is soldered on the connection using standard microstrip technology. The structure is rather similar to the usual quarter-wave electrodes, but more easily constructed. However, it depends on the UHV requirements, whether a suitable dielectric can be found. For a mathematical analysis of planar loops, refer to Ref. [14].

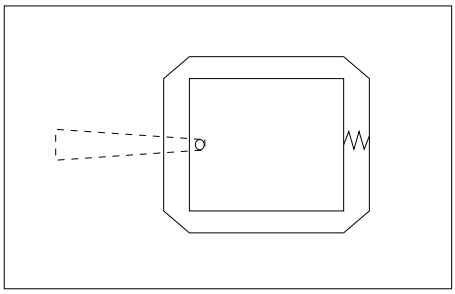

Fig. 5: Schematic view of a planar loop structure.

2.5 Slotted structures

In a slotted structure, a rectangular waveguide is coupled to the vacuum chamber by a regular array of slots (see Fig. 6). The effect of the slots is not only to couple the beam to the structure, but it also decreases the wave velocity inside the waveguide. The addition of an internal conductor transforms the waveguide into a coaxial line. Such devices were conceived by L. Faltin at CERN in the 1970's [15]. At Fermilab, slotted waveguides are used in the 4–8 GHz debuncher upgrade [16]. For a discussion of these and other structures, the reader is referred to C.S. Taylor's lecture on the same subject at the first CAS [7].

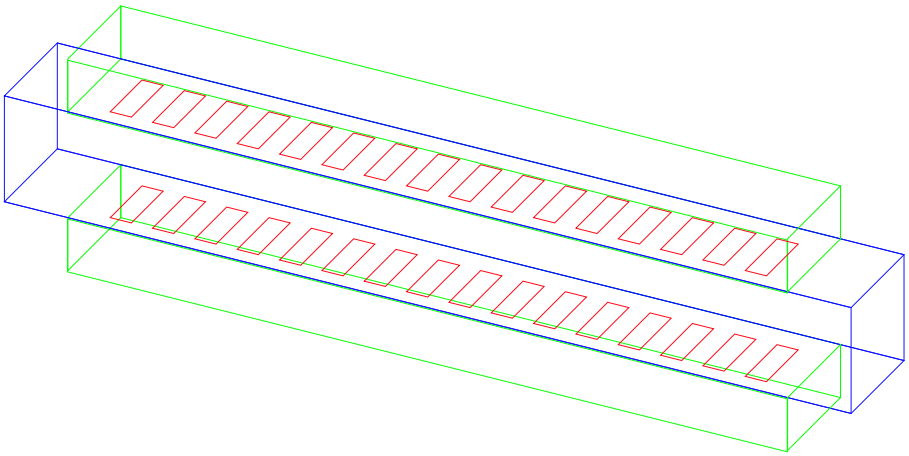

Fig. 6: Schematic view of a slotted waveguide. By inserting an inner conductor inside the waveguide, the principal layout of a Faltin type structure arises.

2.6 Signal combination

Whenever distributed pick-up or kicker structures such as striplines or planar loops are used in stochastic cooling systems, the sensitivity of one such element is seldom sufficient in practice. Therefore one uses several electrodes connected to standard microwave power combiners in order to increase the signal-to-noise ratio on the pick-up side, and the efficiency of turning power into accelerating voltage on the kicker side. A schematic view is shown in Fig. 7. The length of the connecting cables must be adapted

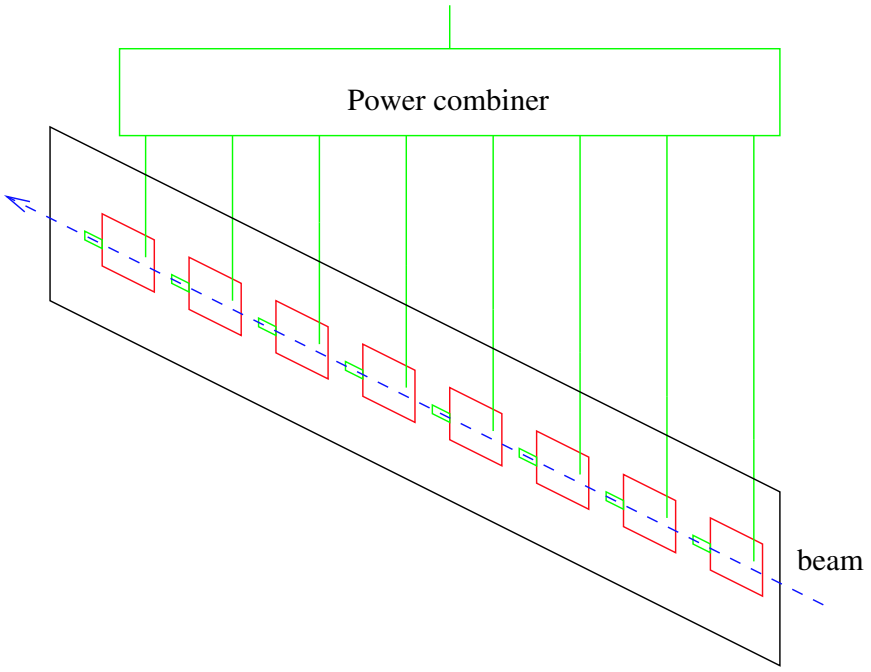

Fig. 7: Schematic view of power combination from distributed pick-up electrodes.

to the beam velocity in order to yield a synchronous addition for signals from the individual pick-ups. Neglecting losses, the output voltage of an n-fold power combiner is

$$V_{\text{out}} = \frac{1}{\sqrt{n}} \sum_{j=1}^{n} V_j \ , \tag{29}$$

where the V_j are the voltages at the input ports. The average power is

$$P_{\text{out}} = \frac{1}{nZ_{\text{line}}} \sum_{j,k=1}^{n} \langle V_j V_k \rangle \ . \tag{30}$$

If the cable lengths are adjusted correctly, the input voltages are equal and one gets $P_{\text{out}} = nP_{\text{single}}$, where P_{single} is the beam power from a single pick-up electrode. But the noise voltages from the individual terminating resistors, V_j and V_k, are uncorrelated for $j \neq k$, and there is no increase of the output noise power in comparison to the individual noise. (This would violate the second law of thermodynamics!.) Therefore one gets an optimum increase of the signal-to-noise ratio by a factor n.

3 RECIPROCITY

Pick-ups and kickers are usually constructed in the same way. This makes sense because of reciprocity. The reciprocity theorem of antenna theory can be proved directly from Maxwell's equations. For this proof, the reader is referred to Ref. [10]. Here we limit ourselves to the physical contents of the theorem. This refers to a given volume with 'metallic' boundaries on which the tangential electric field is

perpendicular to the magnetic field. The pick-up case is treated with fields $\vec{E}_p$, $\vec{H}_p$ and a beam current density $\vec{j}_p$. Fields $\vec{E}_k$ and $\vec{H}_k$ apply to the kicker, and there is no driving current density in this case. The connection between the pick-up and kicker fields is only given by the fact that they rely on equal boundaries. For illustrative purposes, imagine a geometry as in Fig. 8. This figure is adapted from Ref. [10]. The boundaries are sketched by thick lines, there are open surfaces $S_1 \ldots S_4$ for the signal and terminating resistors, and the surfaces S_{c1}, S_{c2} symbolize the boundary between the 'electrode' and the the rest of the vacuum chamber. The reciprocity theorem, stated as an integral equation, relates the pick-up and kicker fields by

$$\int_{\partial\mathcal{V}} dS \left(\vec{E}_p \times \vec{H}_k - \vec{E}_k \times \vec{H}_p \right) = \int_{\mathcal{V}} \vec{E}_k \cdot \vec{j}_p \ . \tag{31}$$

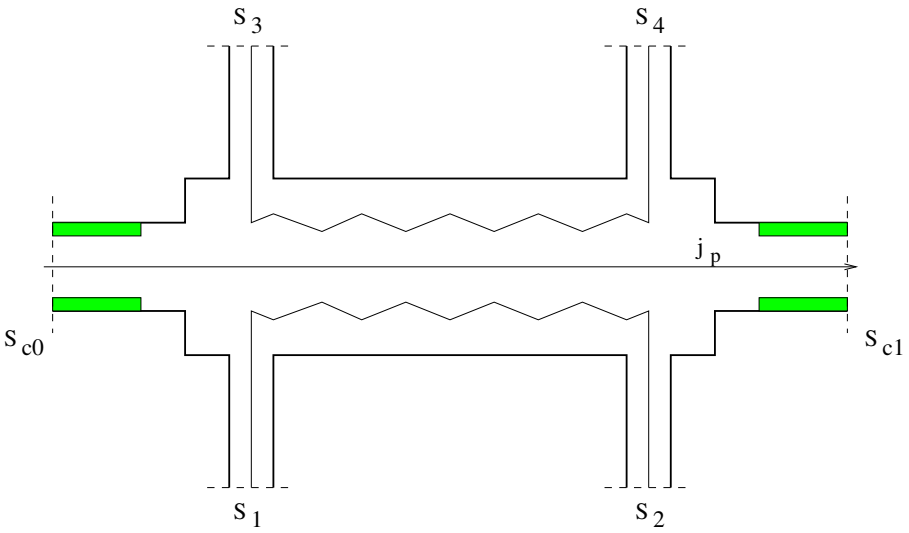

Fig. 8: Schematic view of a pick-up or kicker structure relevant to the discussion of reciprocity.

In this equation, $\mathcal{V}$ is the volume bounded by $\partial\mathcal{V}$. So far everything can be derived strictly from Maxwell's equations. The surface integrand on the left-hand side of Eq. (31) vanishes everywhere except on the open surfaces described above.

An important assumption is that the vacuum chamber boundaries S_{c1} and S_{c2} can be placed so far away from the electrode that their contribution to the surface integral can be neglected. If these propagating modes are damped by attenuating material inside $\mathcal{V}$, the contribution of the vacuum chamber modes is negligible, too. Dampers of this kind are symbolized by the filled areas at the ends of the structure in Fig. 8. The second assumption is that the fields at the ports $S_1 \ldots S_4$ can be described by TEM waves, as they exist in coaxial cables. Then the fields can be desribed using RF voltages V_k or V_p. In Ref. [10] it is shown that in certain circumstances where an outcoming wave $\vec{E}_k$ and an incoming wave $\vec{E}_p$ are considered, the reciprocity theorem can be reduced to the equation

$$V_p(\Omega) = \frac{-Z_{\text{line}}}{2V_k(\Omega)} \int_{\mathcal{V}} \vec{E}_k(x,y,s,\Omega) \cdot \vec{j}_p(x,y,s,\Omega) \ , \tag{32}$$

where Z_{line} is the line impedance of the coaxial line. We shall show that Eq. (32) can be related to the definition of sensitivity in Eqs. (5) and (6). The point-like current density of a single particle on the right-hand side of Eq. (32) can be represented by delta functions:

$$\vec{j}_p(x,y,s,t) = e\vec{v}\delta(x-x_0)\delta(y-y_0)\delta(s-s_0-\beta ct) \ . \tag{33}$$

We have assumed that $\vec{v}$ points essentially in the s direction and that the change in x and y can be neglected during the flight of the particle through the structure. Equation (33) describes just a single passage. In Eq. (32), we need the Fourier transform of the current density:

$$\vec{j}_p(x, y, s, \Omega) = e\frac{\vec{v}}{v}\delta(x - x_0)\delta(y - y_0) \exp\left(\frac{-i\Omega\,(s - s_0)}{v}\right) . \tag{34}$$

The integral on the right-hand side of Eq. (32) yields

$$\int_{\mathcal{V}} \vec{E}_k(x, y, s, \Omega) \cdot \vec{j}_p(x, y, s, \Omega) = \int ds E_{k,s}(x_0, y_0, s, \Omega) \exp\left(\frac{-i\Omega\,(s - s_0)}{v}\right) . \tag{35}$$

This is the Fourier transform of

$$\int ds E_{k,s}\left(x_0, y_0, s, t - \frac{s - s_0}{v}\right) .$$

Comparing with Eq. (5) and using the Fourier convolution theorem, we conclude that

$$V_p(\Omega) = \frac{-qeZ_{\text{line}}}{2} S_{\parallel}(x_0, y_0, \Omega) . \tag{36}$$

This equation shows that the sensitivity we defined in Eq. (3) to describe the action of a kicker is also useful for the description of pick-ups, if both are built identically. The factor 2 in the denominator can be explained qualitatively in the following way: A kicker is usually excited by a counterpropagating wave. On the other hand, a particle passing through a pick-up produces waves in both directions, of which only one is used because of the need to synchronize the wave with the particle velocity.

In the time domain, the signal due to a single passage of the particle is, according to Eq. (36):

$$V_p(t) = \frac{-qeZ_{\text{line}}}{2} S_{\parallel}(x_0, y_0, t) . \tag{37}$$

We shall use this result in the following chapter. An approach to reciprocity, where far-fields are also taken into account, was presented by F. Caspers and G. Dôme in Ref. [17].

4 SIGNAL FROM A CIRCULATING BEAM

4.1 Simplified one-particle signal

In Eq. (36) we have learned how to calculate the pick-up spectrum for a single passage through the device. In a beam coasting in a storage ring, each particle passes through the pick-up periodically. In order to get an easy-to-use mathematical description, we approximate the particle arrival at the pick-up by an infinite train of delta functions:

$$f(t) = \sum_{n=-\infty}^{\infty} \delta\left(t - t_0 - nT\right) . \tag{38}$$

Here t_0 denotes the time of arrival at revolution number $n = 0$. This time is different for each particle in the beam. T is the revolution time, which is normally distributed around a mean revolution time with a certain spread which is proportional to the momentum spread of the beam. The Fourier spectrum of $f(t)$ is also an infinite train of delta functions, but this time in the frequency domain:

$$f(\Omega) = \omega_{\text{rev}} \sum_{m=-\infty}^{\infty} \exp\left(i\Omega t_0\right) \delta\left(\Omega - m\omega_{\text{rev}}\right) , \tag{39}$$

where $\omega_{\mathrm{rev}} = 2\pi/T$ is the (angular) revolution frequency. The time t_0 is expressed by a phase in the spectrum. In order to understand the Fourier pair in Eqs. (38) and (39) properly, it helps to note that the infinite number of frequencies in Eq. (39) is due to the infinitely sharp pulses in the time domain. The reader who is interested in what happens if one or both of these idealized assumptions are dropped, may find it interesting to follow Feynman's rule 'The same equations have the same solutions', and re-examine a well-known analogy in optics: the diffraction pattern of a diffraction grating, which is the Fourier transform of the optical transmission function of the grating. In our case, the number of diffraction slits is mapped to the number of revolutions, whereas the role of the transmission through a single slit is played by the sensitivity $S(x, y, t)$. Working out the details of the analogy is left as an exercise to the reader.

The signal of a pickup with a circulating particle can be modeled in the time domain as the convolution of $f(t)$ with Eq. (37). Therefore the spectrum of a single circulating particle becomes:

$$V_p(\Omega) = \frac{-qeZ_{\mathrm{line}}\omega_{\mathrm{rev}}}{2} \sum_{m=-\infty}^{\infty} \exp\left(i\Omega t_0\right) S_{\|}(x_0, y_0, \Omega)\delta\left(\Omega - m\omega_{\mathrm{rev}}\right) \ . \tag{40}$$

The spectrum consists of sharp lines at each harmonic of the revolution frequency, with an amplitude that is given by the sensitivity, and a phase that depends on the position of the particle.

4.2 One-particle signal including betatron motion

In deriving Eq. (40) we have tacitly assumed that at each revolution, the particle passes through the pick-up at the same position in x and y. However, this assumption does not hold in general, because particles in a storage ring perform betatron oscillations. The pick-up produces a stroboscopic view of these oscillations because it does not observe the transverse motion directly, but can detect the position only revolution by revolution. The position at the nth revolution can be written

$$x_n = x_0 + A_x \sin\left(2\pi n Q_x + \mu_x\right) \tag{41}$$

$$y_n = A_y \sin\left(2\pi n Q_y + \mu_y\right) \ . \tag{42}$$

The quantities A_x and A_y denote the amplitude of the oscillations, and the quantities Q_x and Q_y are the number of oscillations per turn, a very important quantity for the beam dynamics in a storage ring. μ_x and μ_y quantify the phase of the oscillation during revolution number $n = 0$. Usually the beam is centred with respect to the electrode, but in the case of horizontal motion there can be a systematic shift x_0 which is caused by the fact that the particle momentum differs from the design momentum. This effect is called dispersion. For the vertical motion, the effect of dispersion can usually be neglected. In order to calculate the pick-up spectrum with arbitrary sensitivity $S(x, y, t)$ including betatron motion, there is an elegant mathematical method [10]. It begins with a wavelength decomposition of $S_{\|}$, i.e. we calculate the spatial Fourier transform of $S_{\|}$:

$$\tilde{S}_{\|}(k_x, k_y, t) = \int dx\, dy\, S_{\|}(x, y, t)\, e^{-i(k_x x + k_y z)} \tag{43}$$

or, alternatively

$$S_{\|}(x, y, t) = \frac{1}{(2\pi)^2} \int dk_x\, dk_y\, \tilde{S}_{\|}(k_x, k_y, t)\, e^{i(k_x x + k_y y)} \ . \tag{44}$$

The advantage of this representation is that the oscillating quantities x and y appear in an exponential, which can be developed in a series of Bessel function, using the well-known identity familiar to RF engineers from the spectrum of a frequency-modulated signal:

$$\exp(ia\sin x) = \sum_{l=-\infty}^{\infty} J_l(a)\, e^{ilx} \ .$$

Inserted in Eq. (44), this yields

$$S_{\|}(x_n, y_n, t) = \sum_{l_x=-\infty}^{\infty} \sum_{l_y=-\infty}^{\infty} S_{\|}^{(lx,ly)}\left(A_x, A_y, t\right) \exp\left[2\pi i n \left(l_x Q_x + l_y Q_y\right)\right] \tag{45}$$

with the important sensitivity coefficients

$$S_{\|}^{(lx,ly)}\left(A_x, A_y, t\right) = \frac{1}{(2\pi)^2} \int_{-\infty}^{\infty} dk_x\, dk_y\, J_{l_x}\left(k_x A_x\right) J_{l_y}\left(k_y A_y\right) \tilde{S}_{\|}(k_x, k_y, t) e^{ik_x x_0 + i(l_x \mu_x + l_y \mu_y)} \,. \tag{46}$$

These coefficients depend only on constants of the motion and on time.

Let us derive the signal from a single circulating particle. Using the reciprocity theorem Eq. (37) and the pulse train from Eq. (38) yields:

$$V_p(t) = \frac{-qeZ_{\text{line}}}{2} \sum_{l_x=-\infty}^{\infty} \sum_{l_y=-\infty}^{\infty} S_{\|}^{(lx,ly)}\left(A_x, A_y, t\right) \exp\left[2\pi i n \left(l_x Q_x + l_y Q_y\right)\right] * f(t) \,. \tag{47}$$

The exponential in Eq. (47) produces a modulation of the delta peaks in $f(t)$, which leads to a new sequence of sidebands. Indeed, if we insert $f(t)$ from Eq. (38) and transform the exponential in Eq. (47) according to

$$\begin{aligned} &\sum_{n=-\infty}^{\infty} S_{\|}^{(lx,ly)}\left(A_x, A_y, t\right) \exp\left[2\pi i n \left(l_x Q_x + l_y Q_y\right)\right] * \delta(t - nT - t_0) \\ = &\sum_{n=-\infty}^{\infty} S_{\|}^{(lx,ly)}\left(A_x, A_y, t - t_0\right) * \exp\left[i\omega_{\text{rev}} t \left(l_x Q_x + l_y Q_y\right)\right] \delta(t - nT) \,, \end{aligned}$$

then the Fourier transform of this expression becomes

$$\omega_{\text{rev}} \sum_{m=-\infty}^{\infty} S_{\|}^{(lx,ly)}\left(A_x, A_y, \Omega\right) e^{i\Omega t_0} \delta\Big(\Omega - \omega_{\text{rev}}\left(m + l_x Q_x + l_y Q_y\right)\Big)$$

with the spectral coefficients

$$S_{\|}^{(lx,ly)}\left(A_x, A_y, \Omega\right) = \int_{-\infty}^{\infty} dt\, S_{\|}^{(lx,ly)}\left(A_x, A_y, t\right) e^{-i\Omega t} \,. \tag{48}$$

Therefore the spectrum consists of lines at each revolution harmonic with a series of betatron sidebands at a distance $\left(l_x Q_x + l_y Q_y\right) \omega_{\text{rev}}$:

$$V_p(\Omega) = \sum_{m=-\infty}^{\infty} \sum_{l_x=-\infty}^{\infty} \sum_{l_y=-\infty}^{\infty} V_{m,l_x,l_y}(\Omega)\, \delta\left(\Omega - \omega_{\text{rev}}\left(m + l_x Q_x + l_y Q_y\right)\right) \tag{49}$$

$$V_{m,l_x,l_y}(\Omega) := \frac{-qeZ_{\text{line}}\omega_{\text{rev}}}{2} S_{\|}^{(lx,ly)}\left(A_x, A_y, \Omega\right) \exp\left(i\Omega t_0\right) \,. \tag{50}$$

This is the general expression for a pick-up with arbitrary sensitivity including betatron motion. Equations (49) and (50) resemble the simplified expression [Eq. (40)], except that the sensitivity has been replaced by the more complicated coefficients [Eq. (46)], and that all the betatron sidebands have emerged.

In order to see how the formalism presented above works, let us investigate Eq. (46) for the case where the betratron amplitudes A_x, A_y are small compared to the physical dimensions of the electrode. The Fourier transform $\tilde{S}(k_x, k_y, t)$ is negligible for large wave numbers $k = 2\pi/\lambda$ where the wavelength λ is much smaller than these physical dimensions. Therefore only small arguments $k_x A_x$ and $k_y A_y$ of

the Bessel functions contribute significantly to Eq. (46), and we can use the approximation $J_l(w) \approx w^l/(2^l l!)$. This yields factors k^l in front of the $\tilde{S}$ in Eq. (46). Using Eq. (A.1.7), we get the approximate coefficients

$$S_{\|}^{(lx,ly)}(A_x, A_y, \Omega) \approx \frac{A_x^{l_x} A_y^{l_y}}{(2i)^{l_x+l_y}\, l_x!\, l_y!} e^{i(l_x\mu_x + l_y\mu_y)} \left.\frac{\partial^{l_x}\partial^{l_y} S(x,y,\Omega)}{\partial x^{l_x}\partial z^{l_y}}\right|_{x=x_0,y=0}, \quad l_x \geq 0, l_y \geq 0\,. \tag{51}$$

For negative indices, there is a general relation that follows from the properties of the Bessel functions:

$$S_{\|}^{(-l_x,l_y)} = (-1)^{l_x} S_{\|}^{(lx,ly)}, \; S_{\|}^{(l_x,-l_y)} = (-1)^{l_y} S_{\|}^{(lx,ly)}\,. \tag{52}$$

In particular, we get the approximate amplitudes at the revolution harmonics and the first betatron sidebands

$$V_{m,0,0}(\Omega) \approx \frac{-qeZ_{\text{line}}\omega_{\text{rev}}}{2} e^{i\Omega t_0} S(x_0, 0, \Omega) \tag{53}$$

$$V_{m,\pm1,0}(\Omega) \approx \frac{\mp qeZ_{\text{line}}\omega_{\text{rev}} A_x}{4i} e^{i\Omega t_0 \pm i\mu_x} \left.\frac{\partial S(x,y,t)}{\partial x}\right|_{x=x_0,y=0} \tag{54}$$

$$V_{m,0,\pm1}(\Omega) \approx \frac{\mp qeZ_{\text{line}}\omega_{\text{rev}} A_y}{4i} e^{i\Omega t_0 \pm i\mu_y} \left.\frac{\partial S(x,y,t)}{\partial y}\right|_{x=x_0,y=0}\,. \tag{55}$$

In the case of small betatron amplitudes, we have rediscovered Eq. (40) for the signal at the revolution harmonics. The signal at the horizontal [Eq. (54)] and vertical [Eq. (55)] betatron sidebands is proportional to the betatron amplitude and the slope of the sensitivity.

After having shown that the general expression for the sensitivity coefficients, Eq. (46), yields rather simple expressions in the case of small betatron amplitudes, we recall how the coefficients $S_{\|}^{(lx,ly)}$ are calculated in general:

1. Take the spatial Fourier transform $\tilde{S}$ of the sensitivity.
2. Multiply by the weights $J_{l_x}(k_x A_x)$ and $J_{l_y}(k_y A_y)$.
3. Calculate the inverse transform at the point $x = x_0, y = 0$.
4. Take into account the initial betatron phases μ_x and μ_z.

The coefficients $S_{\|}^{(lx,ly)}$ are a generalization of the approximate relations Eqs. (53)–(55) to the case that the betatron motion becomes so large that it begins to feel the non-linearities of the sensitivity. Indeed, it can be shown that Eqs. (53)–(55) are exact if the sensitivity is linear. As the formalism relies on Fourier transforms, it will be easy to implement on a computer as soon as useful sensitivity models are available. It is useful for the geometrical design of the electrodes. During the design procedure, the aim will be to produce reasonable sensitivities even for the largest betatron amplitudes expected.

It can be seen from Eq. (51) that the signals at the higher-order sidebands $|l_{x,y} \geq 2|$ are directly proportional to higher derivatives of the sensitivity and higher powers of the betatron amplitude. For the practical application of stochastic cooling, they should never play a role. However, they are observed (for example at GSI) in spectra of beams with collective transverse instabilities.

4.3 Spectral density and total power

4.3.1 Schottky signal

The total signal from the beam is the superposition of the single particle signal, Eq. (49), of all particles circulating in the storage ring. It is very important to distinguish between bunched beams and coasting beams. Here we treat only the latter, because stochastic cooling is only switched on after the injected beam has been debunched.

In a coasting beam the particles are distributed randomly. This randomness holds for the time t_0 [compare Eq. (38)] which measures the particle position during a given revolution, and the initial betatron

phases μ_x and μ_z [see Eqs. (41) and (42)]. The distribution in $\omega_{\rm rev}$, and in the betatron amplitudes A_x and A_y at the pick-up, can be expressed by a distribution function $\Psi(\omega_{\rm rev}, A_x, A_y)$ which is normalized to the number of particles N in the ring. Because the signal consists of contributions with random phases due to t_0, μ_x and μ_z, the output voltage from a pick-up disappears on the average, but fluctuates around zero. Therefore the average power is non-zero.

The signal from a coasting beam is called a Schottky signal. In 1918 W. Schottky published a paper [18] in which he showed that the current in semiconductors is never exactly constant, but that there are statistical fluctuations which he attributed to the fact that the current consists of individual electrons with a finite elementary charge that are randomly distributed.

The signal from the beam fluctuates, as well. We pointed out in the introduction to this paper that these fluctuations are the very basis of stochastic cooling. In order to describe the signal quantitatively, we briefly recall some common definitions of signal theory [19].

4.3.2 Basic definitions from signal theory

The Schottky signal from a coasting beam is a stochastic voltage $V(t)$. It is characterized statistically by its autocorrelation function, which is defined as the expectation value of the product of V at times t and $t+\tau$. $V(t)$ is a representative of a *stationary* process because the autocorrelation function does not depend on t (This is no longer true for a bunched beam!). Therefore the autocorrelation can be written in the form

$$\langle V(t)\, V(t+\tau)\rangle = R(\tau)\ . \tag{56}$$

The spectral density C is the Fourier transform of the autocorrelation function

$$C(\Omega) = \int_{-\infty}^{\infty} d\tau\, R(\tau) e^{-i\Omega\tau}\ . \tag{57}$$

One should bear in mind that C is defined as a *voltage* density. For a stationary process the Wiener-Khintchine-Theorem holds:

$$\left\langle \tilde{V}(\Omega)\, \tilde{V}^*(\Omega')\right\rangle = 2\pi\, C(\Omega)\, \delta(\Omega-\Omega')\ . \tag{58}$$

In this notation, $\tilde{V}(\Omega)$ is the Fourier transform of $V(t)$ and * denotes the complex conjugate.

The average total electric power is

$$< P >= \frac{1}{Z_{\rm line}} \left\langle V(t)^2\right\rangle = \frac{R(0)}{Z_{\rm line}} = \frac{1}{2\pi Z_{\rm line}} \int_{-\infty}^{\infty} d\Omega\, C(\Omega)\ . \tag{59}$$

4.3.3 Schottky spectral density

The Schottky spectral density C_p at the output port of a pick-up electrode can be derived from the single particle signal Eq. (49) using the distribution Ψ and the assumption of a smooth distribution in t_0, μ_x and μ_y, as discussed above. In Eq. (49) we saw that each particle produces signals at frequencies

$$\Omega = (m + l_x Q_x + l_y Q_y)\, \omega_{\rm rev}\ . \tag{60}$$

The mathematical description of the power density can be complicated due to the possibility of Schottky band overlap. Let us call the maximum width of the distribution in revolution frequencies $\Delta\omega_{\rm rev}$. Then, if $m\Delta\omega_{\rm rev}/\omega_{\rm rev} > 1$, the extreme parts of the frequency distributions begin to overlap for neighbouring harmonics. Already, at lower harmonics, betatron sidebands overlap with revolution harmonics, and with one another.

To be complete, it should be noted that in the following we neglect chromaticity, which would introduce a correlation between ω_{rev} and Q_x or Q_y. For the Schottky power density, we get

$$C(\Omega) = \sum_{m,l_x,l_y} \int dA_x dA_y \Psi \left(\frac{\Omega}{|m + l_x Q_x + l_y Q_y|}, A_x, A_y \right) \left| V_{m,l_x,l_y}(\Omega) \right|^2 . \tag{61}$$

The sum has to be taken over all bands that contribute to Ω and one has to integrate over betatron amplitudes. Let us derive from Eq. (61) some useful approximations. If

1. the approximation Eq. (53) holds for all betatron amplitudes, and
2. if $S_{m,0,0}$ does not depend on ω_{rev}, and
3. Schottky bands do not overlap,

then the following proportionality holds for the integrated power $P_{m,0,0}$ over one band at harmonic m:

$$P_{m,0,0} \propto N q^2 . \tag{62}$$

Under these assumptions, the Schottky power in one band is proportional to the number of particles and to the square of the charge state. It can serve to measure the beam current, if it is properly calibrated. Obviously, the signal-to-noise ratio of heavy ion beams is intrinsically much higher than for singly charged particle beams, if one assumes identical electrodes and the same number of particles. The signal from a beam of fully stripped uranium ions is 39 dB higher than the one from a corresponding (anti)proton beam.

For the power in the betatron sidebands $P_{m,\pm1}$ there is a similar relation if one assumes $S_{m,\pm1,0}$ or $S_{m,0,\pm1}$ to be constant and that they can be described by Eq. (54) or Eq. (55), respectively:

$$P_{m,1,0} \propto N q^2 \left\langle A_x^2 \right\rangle \tag{63}$$
$$P_{m,0,1} \propto N q^2 \left\langle A_y^2 \right\rangle . \tag{64}$$

The integrated sideband power is therefore a useful diagnostic for the mean betatron amplitude.

4.3.4 Noise spectral density

The noise power of a source at temperature T_{eff} in a frequency interval Δf can be approximated by

$$P_{\mathrm{noise}} = k_{\mathrm{B}} T_{\mathrm{eff}} \Delta f . \tag{65}$$

The noise spectral density C_{noise} inside Δf is constant:

$$C_{\mathrm{noise}}(\Omega) = \frac{1}{2} Z_{\mathrm{line}} k_{\mathrm{B}} T_{\mathrm{eff}} . \tag{66}$$

The factor $1/2$ stems from the necessity to integrate over both positive and negative values of Ω, when one deals with Fourier transforms.

4.4 Transverse pick-up designs

For a good betatron signal the sensitivity should be zero for a centred beam and approximately linear up to the highest betatron amplitudes to be expected [compare Eqs. (54) and (55)]. A vertical pick-up, for example, could consist of two stripline electrodes operated in the difference mode. A horizontal pick-up would be obtained by turning this device around by $90°$. If large horizontal apertures are required, a more effective solution consists of two pairs of stripline electrodes. Each pair is operated in the sum mode, and then one takes the difference of the sum signals. Such a geometry is sketched in Fig. 9.

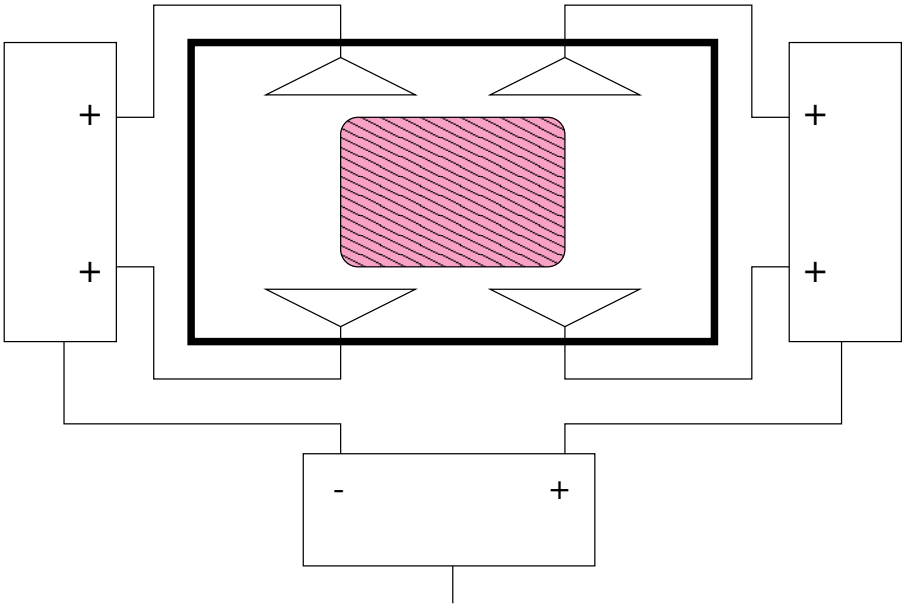

Fig. 9: Schematic sketch of horizontal pick-up. The useful beam aperture is shaded.

4.5 Momentum signal

4.5.1 General requirements

The momentum correction signal at the kicker should carry information about the deviation δp of the particle momentum from the design momentum p_0. Ideally it should be proportional to $\delta p/p_0$. Two methods have been developed to extract this information. The Palmer method relies on dispersion, whereas the notch filter method operates completely in the frequency domain.

4.5.2 Palmer pick-ups

In the Palmer method, the momentum correction signal is derived from the position of the particle as it passes through the pick-up. The dependence of position on momentum is called dispersion. It can be written in the form

$$x_0 = D\frac{\delta p}{p_0}\,, \tag{67}$$

where D is a quantity measured in metres and is called the dispersion function. It is caused by the fact that the orbit curvature in a dipole magnet is proportional to momentum. In a storage ring, D varies around the ring. Therefore, an appropriate location must be chosen for the Palmer pick-up. Palmer pick-ups are transverse pick-ups like the one shown in Fig. 9. The signal can be described approximately by Eq. (53). The proportionality to $\delta p/p_0$ is caused by the x_0 dependence of the sensitivity. In order to get a clean signal from the device, the horizontal betatron amplitude A_x at the location of the Palmer pick-up should be small compared to the dispersion amplitude x_0.

4.5.3 Thorndahl notch filters

The pick-up for the notch filter method has constant sensitivity. The signal is derived by electronic post-processing. It relies on the fact that the revolution frequency depends on momentum:

$$\frac{\delta\omega_{\rm rev}}{\omega_{\rm rev}} = \eta\frac{\delta p}{p_0}\,, \tag{68}$$

where η is a quantity called frequency dispersion. It is explained in every introductory text on longitudinal beam dynamics, because it is important for the description of what happens to a bunch in an RF

field.

In a notch filter the signal is split in a power splitter. The two components pass a short and a long delay line and are then fed into to a 180° hybrid. If the time difference of the signal transmission in the

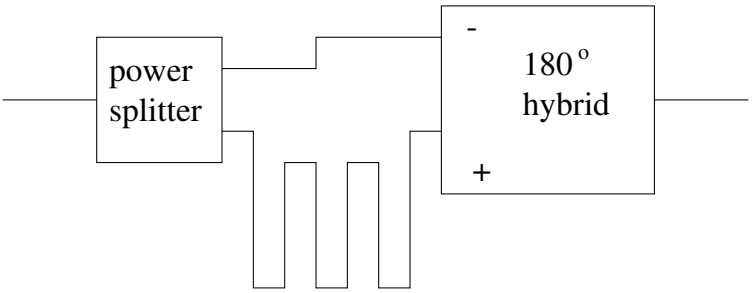

Fig. 10: Schematic sketch of a notch filter.

two cables is t_{notch}, the output voltage will take the form

$$V_0 \left(e^{i\Omega t_{\mathrm{notch}}} - 1\right) = 2iV_0 e^{i\Omega t_{\mathrm{notch}}/2} \sin \frac{\Omega t_{\mathrm{notch}}}{2} \,. \tag{69}$$

If $t_{\mathrm{notch}}/2$ is made equal to the revolution frequency, the transmission will be periodic with the revolution frequency and exhibit zeros at all harmonics of the revolution frequency. This is due to destructive interference between the waves from the short and long cables. These zeros are often called notches. The device is also known as a comb filter. The quality of the cancellations depends on the attenuation of the two waves in the two cables which must be equalized over the whole useful bandwidth. The transmission S_{21} of the notch filters fulfils the requirements of a momentum signal for stochastic cooling in a frequency interval of half a revolution frequency at most. Therefore, the frequency spread of the Schottky signal should be smaller than that at the highest frequency used in the cooling system. The decision to use notch filters in stochastic cooling systems has an important impact on the ion optical design of the cooler ring, because of the constraints on the frequency dispersion η. The appplication of notch filters for momentum cooling was invented by L. Thorndahl and G. Carron at CERN in the 1970s [20]. It played a major role in the successful stochastic cooling of antiproton beams.

An important advantage of notch filters is the suppression of thermal noise around the notches. As the length of the long cable is usually of the order of a few hundred metres, notch filters tend to be sensitive to thermal variations. A modern solution to this problem has been worked out at COSY [21]. They replace the long cable by a fibre-optic, which is connected to an optical modulator and demodulator. The optical devices are less sensitive to thermal variations, and the electric length can be tuned by movable mirrors.

5 TRANSVERSE KICKS

5.1 Panofsky–Wenzel theorem

Transverse kicks to particles moving in an RF field are described by the Panofsky–Wenzel theorem [22]. To every newcomer in the field, this theorem appears to come as a surprise, because it maintains that transverse electric fields are not needed to describe the transverse kick. A proper understanding of the Panofsky–Wenzel theorem is a necessary prerequisite for the design of transverse kicker electrodes. At first we present a straightforward derivation where the electric and magnetic fields are used directly. The equations needed are the Lorentz force equation

$$\frac{d\vec{p}}{dt} = qe\left(\vec{E} + \vec{v} \times \vec{B}\right) \tag{70}$$

and Faraday's law of induction

$$\vec{\nabla} \times \vec{E} = -\frac{\partial \vec{B}}{\partial t} \,. \tag{71}$$

It will soon become clear that the magnetic component of the Lorentz force is as important as the electric one in the derivation. Remember that the fields seen by the particle depend on the space coordinates and on time, i.e. they must be written as $\vec{E}(\vec{r}(t), t)$ and $\vec{B}(\vec{r}(t), t)$. Then the time derivative of the electric field is

$$\frac{d\vec{E}}{dt} = \frac{\partial \vec{E}}{\partial t} + \left(\vec{v} \cdot \vec{\nabla}\right) \vec{E} \,. \tag{72}$$

Because we are dealing with sinusoidally varying fields, we investigate the partial time derivative of the Lorentz force, making use of Eqs. (71) and (72):

$$\begin{aligned} \frac{\partial}{\partial t}\left(\vec{E} + \vec{v} \times \vec{B}\right) &= \frac{\partial \vec{E}}{\partial t} - \vec{v} \times \left(\vec{\nabla} \times \vec{E}\right) \\ &= \frac{\partial \vec{E}}{\partial t} + \left(\vec{v} \cdot \vec{\nabla}\right) \vec{E} - \vec{\nabla}\left(\vec{v} \cdot \vec{E}\right) \\ &= \frac{d\vec{E}}{dt} - \vec{\nabla}\left(\vec{v} \cdot \vec{E}\right) \,. \end{aligned} \tag{73}$$

We assume sinusoidally varying fields $\vec{E} = \vec{E}_0(\vec{r}) \exp i\Omega t + \text{c.c.}$ and $\vec{B} = \vec{B}_0(\vec{r}) \exp i\Omega t + \text{c.c.}$, where c.c. denotes the complex conjugate. With Eq. (73), the integrated change of momentum in a kicker over a length $(s_1 - s_0)$ can be written

$$\Delta\vec{p} = \frac{qe}{i\Omega}\left[\vec{E}(s_1) - \vec{E}(s_0) - \frac{1}{v}\int_{s_0}^{s_1} ds \vec{\nabla}\left(\vec{v} \cdot \vec{E}\right)\right] + \text{c.c.} \tag{74}$$

The velocity change in an RF kicker is usually small, and therefore $\vec{v}$ has been assumed to be approximately constant in the integrand. The entrance and exit points may be moved to a place where the electric field can be neglected. For a kick in the x-direction, Eq. (74) yields

$$\Delta p_x = \frac{iqe}{\Omega v}\int_{s_0}^{s_1} ds \left(v_x \frac{\partial E_x}{\partial x} + v_y \frac{\partial E_y}{\partial x} + v\frac{\partial E_s}{\partial x}\right) + \text{c.c.} \tag{75}$$

In most practical field configurations, the terms $v_x \partial E_x/\partial x$ and $v_y \partial E_y/\partial x$ can be neglected because the velocity points mainly in the s direction. Then

$$\Delta p_x = \frac{i}{\Omega}\frac{\partial \Delta E}{\partial x} \,, \tag{76}$$

where ΔE is the change of energy in the kicker. This relation looks very unfamiliar at first sight. The following comments should clarify the physical meaning of Eq. (76):

- The transverse kicks are proportional to the transverse gradient of the longitudinal electric field.
- No transverse fields are needed for a complete description of the transverse kick.
- Even if a particle passing through a transverse kicker on-axis does not feel an accelerating voltage, off-axis particles do.
- For a given transverse deflection, the necessary transverse field gradient of the longitudinal electric field is proportional to the RF frequency.
- There is a 90° phase difference between the maximum transverse kick and the maximum (off-axis) energy change.
- In the low-frequency limit, the longitudinal electric fields do not play a practical role.
- As Panofsky and Wenzel pointed out in their concise original paper, there can be no transverse deflection in a pure TE field.

Tracing back the derivation of Eqs. (73)–(76), it becomes obvious that the effective transverse kick is produced by a component of the magnetic force. Because of the law of induction, it can be described in terms of the electric field. There is no net effect of the actual electric force because there is a second component of the magnetic force which adds up to the electric field to produce a total time derivative of $\vec{E}$, the effect of which vanishes under suitable boundary conditions.

A more elegant, perhaps somewhat less instructive way to derive the Panofsky–Wenzel theorem makes use of the vector potential $\vec{A}$ and the relations $\vec{E} = -\partial\vec{A}/\partial t$, as well as $\vec{B} = \vec{\nabla} \times \vec{A}$ in the Lorentz force term. Doing so, there is no need to operate with the partial time derivative of the Lorentz force. Instead of terms like $1/(i\Omega)\partial E_s/\partial x$ [see Eq. (75)] the simpler, equivalent terms $\partial A_s/\partial x$ turn up. The reader should try and derive this as an exercise. This is the main reason behind defining the sensitivity via the vector potential in Eq. (2). Definitions in the time domain as Eqs. (7) and (8) would have become too cumbersome without using the vector potential.

It is rewarding to compare the order of magnitude of the transverse kick to the longitudinal kick for off-axis particles. Let the beam be centred with respect to the transverse kick electrode and let the longitudinal kick to particles in the centre vanish. Let the transverse kick be constant inside an aperture Δx. According to the Panofsky–Wenzel theorem, a transverse kick by an angle $\Delta x'$ must be accompanied by an off-axis energy change ΔE. Both are related by

$$\Delta x' = \frac{\Delta p_x}{p_0} = \frac{1}{i\Omega m\beta\gamma c}\frac{\Delta E}{\Delta x} \,. \tag{77}$$

On the other hand,

$$\frac{\Delta E}{m\gamma c^2} = \frac{\Delta E}{E_0} = \beta^2\frac{\Delta p}{p_0} \,. \tag{78}$$

Combining Eqs. (77) and (78) one gets an easy-to-use relation between the transverse and longitudinal kicks:

$$\frac{\Delta p}{p_0} = \frac{i\Omega\Delta x}{\beta c}\Delta x' \,. \tag{79}$$

For $\Omega/2\pi = 1$ GHz, Δx = 10 mm, and $\beta = 1$, we get $\Omega\Delta x/\beta c = 0.2096$, i.e. a kick by 1 mrad would be accompanied by a change in relative momentum of 2×10^{-4} at a beam radius of 10 mm. With Eq. (79) this relation can easily be scaled.

6 BEAM DYNAMICS WITH KICKS

A quantitative description of the beam response to the voltages applied at the kicker(s) is beyond the scope of this lecture because of the complicated beam dynamics involved. At this point, a few general remarks should be sufficient. The reader is advised to consult the literature. As already mentioned, a good introduction can be found in Ref. [1]. The ambitious reader interested in the physics of fluctuating signals should consult Ref. [23].

A particle circulating in the ring can get into resonance with the applied kicker signal. In the long term, it will be most sensitive to signals at the frequencies given by Eq. (60), i.e. at the same frequencies that it produces a signal at a pick-up. For the longitudinal response, the most important effect occurs at the frequencies $m\omega_{\mathrm{rev}}$. It is proportional to the kicker sensitivity $S_{\parallel}^{(0,0)}$. Neglecting the effect of betatron oscillations, this is roughly the quantity $S_{\parallel}$.

The change of the betatron amplitudes occur mainly because of the signal at the betatron sidebands $(m \pm Q_x)\,\omega_{\mathrm{rev}}$ and $(m \pm Q_y)\,\omega_{\mathrm{rev}}$. Because of the Panofsky–Wenzel theorem, it is proportional to $\partial S/\partial x$ and $\partial S/\partial y$ [see Eqs. (7) and (8)].

APPENDIX - FOURIER TRANSFORMS AND NOTATION

The Fourier transform is defined as a transformation between the time domain and the frequency domain. In this paper, we consistently use the definitions from Ref. [19]. Time is denoted by t and angular frequency by Ω. The original function and its Fourier transform are denoted by the same letter, e.g. $V(t)$ and $V(\Omega)$. This is mathematically not quite correct, but saves a lot of nasty indices. A localized exception to this rule is the spatial transform $\tilde{S}$ used in Eqs. (43)–(46). The Fourier transform is defined as

$$f(\Omega) = \int_{-\infty}^{\infty} dt\, f(t) \exp(-i\Omega t) \tag{A.1.1}$$

The Fourier inversion theorem yields

$$f(t) = \frac{1}{2\pi} \int_{-\infty}^{\infty} dt\, f(\Omega) \exp(+i\Omega t) \tag{A.1.2}$$

If $f(t)$ and $f(\Omega)$ are related by a Fourier transform, we write

$$f(t) \leftrightarrow f(\Omega) \tag{A.1.3}$$

The following theorems are used in this paper

1. the linearity theorem
$$af(t) + bg(t) \leftrightarrow af(\Omega) + bg(\Omega) \tag{A.1.4}$$
2. the shift theorem
$$f(t-a) \leftrightarrow f(\Omega) \exp(-i\Omega a) \tag{A.1.5}$$
3. the modulation theorem
$$f(t) \exp(i\omega_0 t) \leftrightarrow f(\Omega - \omega_0) \tag{A.1.6}$$
4. the theorem on derivatives
$$\frac{d^n f(t)}{dt^n} \leftrightarrow (i\Omega)^n f(\Omega) \tag{A.1.7}$$
5. and, perhaps, the most important of them all, the convolution theorem
$$\int_{-\infty}^{\infty} d\tau\, f(t) g(t-\tau) \leftrightarrow f(\Omega) g(\Omega) \tag{A.1.8}$$

The convolution is often written in short-hand form

$$\int_{-\infty}^{\infty} d\tau\, f(t) g(t-\tau) := f(t) * g(t) \tag{A.1.9}$$

A very useful identity concerns the convolution with a delta function

$$\delta(t-a) * g(t) = g(t-a) \tag{A.1.10}$$

Most often the quantities $f(t)$ in the time domain refer to physically measurable quantities , i.e they are represented by real numbers. The negative frequency components of the Fourier transform of a real function $f(t)$ can easily be calculated from the positive frequency components: $f(-\Omega) = f^*(\Omega)$.

REFERENCES

[1] D. Möhl, CERN Report 95–06, 587–664.

[2] R. Stassen, U. Bechstedt, J. Dietrich, K. Henn, A. Lehrach, R. Maier, S. Martin, D. Prasuhn, A. Schnase, H. Schneider, H. Stockhorst, R. Tölle, Proc. EPAC 98, 553–555.

[3] F. Nolden, B. Franzke, A. Schwinn, F. Caspers, Proc. EPAC 98, 1052–1054.

[4] T. Katayama, S. Watanabe, Y. Batygin, N. Inabe, K. Ohtomo, T. Ohkawa, M. Takanaka, T. Tanabe, M. Wakasugi, I. Watanabe, Y. Yano, K. Yoshida, Proc. EPAC 98, 529–531.

[5] R.J. Pasquinelli, Proc. PAC 99, 1094–1096.

[6] G. Carron, F. Caspers, L. Thorndahl, CERN Report 85–01.

[7] C.S. Taylor, CERN Report 92-03, 458–473.

[8] F. Caspers, Proc. Joint-US-CERN-Japan International School on Frontiers of Accelerator Technology, 3–9. Nov. 1994, World Scientific.

[9] G. Lambertson, AIP Conf. Proc. **153** (1987) 1414–1442.

[10] J. Bisognano, C. Leemann, AIP Conf. Proc. **87** (1982) 584–655.

[11] E. Durand, Electrostatique, Tome II, Masson et Cie, Paris 1966.

[12] F. Nolden, K. Beckert, F. Caspers, B. Franczak, B. Franzke, R. Menges, A. Schwinn, M. Steck, Nucl. Instrum. Methods A **441** (2000) 219–222.

[13] P. Raabe, VDI Fortschrittberichte, Reihe 21 (Elektrotechnik), Nr. 128 (1993).

[14] J. Petter, D. McGinnis, J. Marriner, Proc. PAC 89, 636–638.

[15] L. Faltin, Nucl. Instrum. Methods **148** (1978) 449–455.

[16] D. McGinnis, Proc. PAC 99, 1713–1715.

[17] F. Caspers, G. Dôme, Proc. EPAC 94, 1208–1210.

[18] W. Schottky, Ann. Phys **57** (1918) 541.

[19] A. Papoulis, Signal Analysis, McGraw-Hill 1977.

[20] G. Carron, L. Thorndahl, internal report CERN/ISR–RF/78–12.

[21] U. Bechstedt, J. Dietrich, K. Henn, A. Lehrach, R. Maier, D. Prasuhn, A. Schnase, H. Schneider, R. Stassen, H. Stockhorst, R. Tölle, Proc. PAC 99, 1701–1703.

[22] W. Panofsky, W. Wenzel, Rev. Sci. Inst. **27** (1956) 967.

[23] S. Chattopadhyay, CERN 84–11.